Mode coupling in two-dimensional magnetohydrodynamic flows

Nijboer, R.J.; Goedbloed, J.P.

published in
Journal of Plasma Physics
1999

DOI (link to publisher)
10.1017/S0022377898007430

document version
Publisher's PDF, also known as Version of record

J. Plasma Physics (1999), *vol.* 61, *part* 2, *pp.* 241–262. Printed in the United Kingdom

Mode coupling in two-dimensional magnetohydrodynamic flows

R. J. NIJBOER and J. P. GOEDBLOED

FOM–Institute for Plasma Physics Rijnhuizen, Edisonbaan 14, Postbus 1207, 3430 BE Nieuwegein, The Netherlands

(Received 21 July 1998)

The spectrum of incompressible waves and instabilities of two-dimensional plasma geometries with background flow is calculated. The equilibrium is solved numerically by the recently developed program FLow Equilibrium Solver (FLES). The spectra of the equilibria are computed by means of another new program, the INcompressible 2-dimensional FLow Eigenvalue Solver (IN2FLES). Magnetic instabilities and instabilities driven by the two-dimensionality and the flow are found. For linear equilibria, the eigenvalues for elliptical geometries remain close to the curves on which the eigenvalues for circular geometries lie. These curves may be found for unbounded domains by a calculation in Fourier space [see Lifschitz, A. In: *Proceedings of 1995 International Workshop on Operator Theory and Applications* (ed. R. Mennicken and C. Tretter), pp. 97–117, Birkhäuser, Boston, 1998]. Here the relation between a new continuous spectrum of unbounded domains and the discrete spectrum of bounded domains is investigated. Finally, it is found that the two-dimensionality and the background flow may lead to an overstable cluster-point.

1. Introduction

Waves and instabilities in plasmas may be investigated by means of spectral analysis. Over the years, this has been done for both fusion plasmas and astrophysical plasmas. For fusion plasmas, the assumption of a static equilibrium has often been made. However, owing to neutral beam injection or divertor action, the plasma will flow and this assumption is violated. For astrophysical plasmas, the opposite is true. Here the magnetic field has often been neglected. However, it was found that the magnetic field plays a dominant role in the plasma behaviour. Therefore the study of the magnetohydrodynamic spectrum of flowing magnetized plasmas is of interest both for fusion research and for astrophysics.

In this paper, we consider cylindrical plasmas. This geometry may be used as a model for many applications. The cylinder may be seen as a first-order approximation of a toroidal geometry, and hence results of our study are useful for tokamak plasmas and for solar coronal loops. Moreover, cylindrical plasma geometries do occur in astrophysical jets and accretion disks.

The effect of equilibrium flow in circular cylinders has been studied by a number of authors. Suydam modes were considered by Hameiri (1981) and Bondeson et al. (1987). The Kelvin–Helmholtz instability of rotating jets was investigated by, for example, Bodo et al. (1989) and Appl and Camenzind (1992). Finally, we mention

the investigations of accretion disks, where a small magnetic field in combination with a sheared rotation generates an instability that may explain the enhanced turbulence in these disks (Balbus and Hawley 1998).

Our previous investigations of the spectrum of plasmas with closed flux surfaces and equilibrium flow were restricted to one-dimensional equilibria (Nijboer et al. 1997a,b). Results on the spectrum of two-dimensional flow equilibria, however, show that new phenomena may occur. For instance, equilibrium flow in two-dimensional geometries may turn the continuous spectrum overstable. This was shown by Hameiri and Hammer (1979), who considered a cylindrical geometry with longitudinal magnetic field and poloidal flow, and by Hellsten and Spies (1979), who considered a toroidal geometry with toroidal flow and poloidal magnetic field. Nijboer et al. (1998) considered an X-point geometry. A new continuous spectrum was found for unbounded domains. It was shown that the classical continuous spectrum is part of this new continuum. Since the new continuum turns overstable for large poloidal flows, this means that the classical continuum turns overstable as well. Since all calculations were performed completely in Fourier space, the link with physical space is not always transparent. In this paper, this is overcome by calculating the two-dimensional spectrum numerically in physical space.

We discuss the spectrum of two-dimensional incompressible magnetohydrodynamic flows in a cylindrical geometry with non-circular cross-section. We include poloidal and longitudinal components for the equilibrium quantities of both the flow velocity and the magnetic field. Apart from a discussion of the continuous spectrum, we mainly concentrate our study on the discrete part of the spectrum. Owing to the equilibrium flow, the spectral values belonging to overstable and damped modes lie in the complex plane, and they are clearly separated for different poloidal mode numbers. Hence the effects of mode coupling due to a non-circular geometry are easily studied in these situations.

The paper is structured as follows. In Sec. 2, the incompressible equilibrium is discussed. The equilibrium is described by the modified Grad–Shafranov equation, and we find its solutions numerically. In Sec. 3, we consider deviations from equilibrium, and present a numerical code for the calculation of the spectrum. The continuous part of this spectrum is discussed in Sec. 4, and the results on the discrete spectrum are presented in Sec. 5. Conclusions are given in Sec. 6.

2. Flow equilibria

The magnetohydrodynamic equilibrium of a flowing plasma is described by the modified Grad–Shafranov equation and the Bernoulli equation (see e.g. Agim and Tataronis 1985). For a compressible plasma, this means that one has to solve these two coupled equations for the magnetic flux and the poloidal Alfvén Mach number, as is done, for instance, by Goedbloed and Lifschitz (1997). For an incompressible plasma, however, the poloidal Alfvén Mach number and the density profiles become flux functions, and the Bernoulli equation reduces to a definition of a Bernoulli-type of function H, which, for a cylindrical geometry, takes the form (Nijboer et al. 1998)

$$H(\Psi) = P + \tfrac{1}{2}\rho V_p^2 + \tfrac{1}{2}B_z^2. \tag{2.1}$$

Here Ψ denotes the magnetic flux, P the gas pressure, ρ the density, V_p the poloidal flow velocity and B_z the longitudinal magnetic field. This means that only the

modified Grad–Shafranov equation has to be solved for the magnetic flux. This equation reduces to

$$(1 - M^2)\boldsymbol{\nabla} \cdot \boldsymbol{\nabla}\Psi - \tfrac{1}{2}(M^2)'|\boldsymbol{\nabla}\Psi|^2 + H'(\Psi) = 0, \tag{2.2}$$

where $' \equiv d/d\Psi$, $M^2(\Psi) \equiv \rho V_p^2/B_p^2$ is the square of the poloidal Mach number, and B_p is the poloidal magnetic field. The magnetic flux can be determined from (2.2) whenever profiles for the poloidal Alfvén Mach number and the Bernoulli function are given. Apart from the Mach number and the Bernoulli function, there are three more free flux functions, namely the density, the longitudinal magnetic field and the longitudinal velocity V_z. The equilibrium flux, however, does not depend on the latter three profiles.

The modified Grad–Shafranov equation (2.2) is an elliptic differential equation. Since there are no transitions to a hyperbolic regime, shocks will not occur. However, we do have to keep in mind the singularity $M^2 = 1$. Since (2.2) is of the same form as the Grad–Shafranov equation for static compressible plasmas, the same numerical techniques used for solving the Grad–Shafranov equation for static plasmas may be used to find stationary equilibrium states of incompressible flowing plasmas. For that purpose, we adapted the HELENA code (Huysmans et al. 1991), which is restricted to static equilibria. The new code is called FLES (FLow Equilibrium Solver).

Consider a cylindrical plasma with non-circular cross-section. An infinitely conducting wall is taken to be situated at the plasma boundary. General cross-sections can be considered, but we restrict our analysis to up–down-symmetric geometries. The magnetic flux is scaled as

$$\psi = \frac{\Psi - \Psi_0}{\Psi_1 - \Psi_0}, \tag{2.3}$$

such that $0 \leqslant \psi \leqslant 1$. Here Ψ_1 is the flux at the boundary and Ψ_0 the flux at the magnetic axis. Furthermore, the coordinates are scaled with a lengthscale L such that $-1 \leqslant x \leqslant 1$. For an example of the scaled cross-section, see Fig. 1.

The Galerkin method in combination with a finite-element method is used to find solutions. The coordinates x and y and the magnetic flux ψ are discretized with bicubic Hermite elements. This allows an accurate representation of $\psi(x, y)$ where both ψ and $\boldsymbol{\nabla}\psi$ are continuous across element boundaries. Equation (2.2) is put into the weak form

$$\int V_i \boldsymbol{\nabla} \cdot \boldsymbol{\nabla}\psi \, d\mathbf{x} = \int V_i \left[\frac{1}{2} \frac{(M^2)'}{1 - M^2} |\boldsymbol{\nabla}\psi|^2 - \frac{\bar{H}'}{1 - M^2} \right] d\mathbf{x}. \tag{2.4}$$

Here V_i is a test function that is chosen from the set of Hermite elements. The prime is redefined as $' \equiv d/d\psi$. The function $\bar{H}$ is a new dimensionless profile, defined as

$$\bar{H}(\psi) = \frac{L^2}{(\Psi_1 - \Psi_0)^2} H(\Psi). \tag{2.5}$$

The boundary conditions $\psi = 1$ at the plasma–wall boundary and $\boldsymbol{\nabla}\psi \cdot \mathbf{n}$ at the axis of symmetry are implemented as natural boundary conditions.

After discretization of x, y and ψ with bicubic Hermite elements, (2.4) gives a system of equations

$$K\psi_{n+1} = \mathbf{b}(\psi_n), \tag{2.6}$$

with

$$K_{ij} = \int V_i \boldsymbol{\nabla} \cdot \boldsymbol{\nabla} V_j \, d\mathbf{x}, \tag{2.7}$$

$$b_i = \int V_i \left[\frac{1}{2} \frac{M^2(\psi_n)'}{1 - M^2(\psi_n)} |\boldsymbol{\nabla}\psi_n|^2 - \frac{\bar{H}'(\psi_n)}{1 - M^2(\psi_n)} \right] d\mathbf{x}. \tag{2.8}$$

ψ_n is a vector containing an approximation of the discretized magnetic flux. The $\bar{H}'$ profile is made independent of amplitude by introducing a new profile $\hat{H}'$:

$$\bar{H}'(\psi) = A\hat{H}'(\psi), \tag{2.9}$$

such that $A = \bar{H}'(0)$ and $\hat{H}'(0) = 1$.

The system (2.6) can then be solved using a Picard iteration. The approximation of the magnetic flux at iteration step $n + 1$ is determined from the approximation at step n by inverting the matrix $\mathbf{K}$. Note that, since the term $1 - M^2$ has been brought to the right hand side, the matrix $\mathbf{K}$ is constant and hence need only be inverted once during the iteration process. In order for this iteration process to converge, the right-hand side of (2.6) must be smaller in norm than 1. Therefore the profile for M must not pass $M = 1$, and the profiles for $(M^2)'$ and $\hat{H}'$ must not become too large. The global parameter A and the position of the magnetic axis are eigenvalues that are determined together with the solution ψ in the iteration process.

When the solution is found, it is mapped onto a flux coordinate sytem defined by the following co- and contravariant basis vectors:

$$\mathbf{u}^1 = \boldsymbol{\nabla}\psi, \qquad \mathbf{u}_1 = J\boldsymbol{\nabla}\vartheta \times \boldsymbol{\nabla} z, \tag{2.10a}$$

$$\mathbf{u}^2 = \boldsymbol{\nabla}\vartheta, \qquad \mathbf{u}_2 = J\boldsymbol{\nabla} z \times \boldsymbol{\nabla}\psi, \tag{2.10b}$$

$$\mathbf{u}^3 = \boldsymbol{\nabla} z, \qquad \mathbf{u}_3 = J\boldsymbol{\nabla}\psi \times \boldsymbol{\nabla}\vartheta, \tag{2.10c}$$

where $0 \leqslant \psi \leqslant 1$ and J is the Jacobian of the (ψ, ϑ, z) coordinate system. In these coordinates, the equilibrium magnetic field and velocity take the forms

$$\mathbf{B}_0 = \frac{1}{J}\mathbf{u}_2 + B_z(\psi)\mathbf{u}_3, \tag{2.11a}$$

$$\mathbf{V}_0 = \frac{M(\psi)}{[\rho(\psi)J]^{1/2}}\mathbf{u}_2 + V_z(\psi)\mathbf{u}_3. \tag{2.11b}$$

The coordinate ψ and the Jacobian J follow from the equilibrium solution. The coordinate ϑ will be constructed from this solution in such a way that magnetic field lines become straight lines. This allows an easy representation of the operators $\mathbf{B}_0 \cdot \boldsymbol{\nabla}$ and $\mathbf{V}_0 \cdot \boldsymbol{\nabla}$, that arise in the calculation of the spectrum of these equilibria.

We introduce a magnetic winding number ν, which is related to the safety factor for toroidal geometries by

$$\nu = \frac{B^3}{B^2} = JB_z(\psi). \tag{2.12}$$

The winding number gives the increase in the longitudinal (z) direction for a change in the poloidal (ϑ) direction along a magnetic field line:

$$\left.\frac{dz}{d\vartheta}\right|_{\text{field line}} = \nu. \tag{2.13}$$

Going once along the poloidal direction gives a total increase in z of $Z(\psi)$. Hence

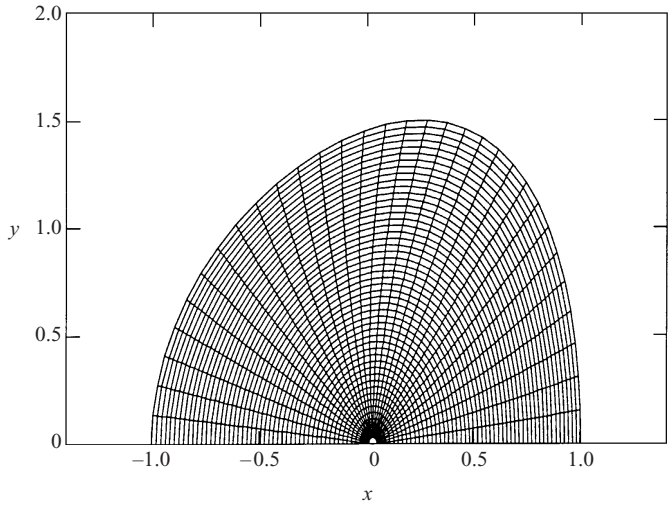

Figure 1. Flux surfaces and equidistant ϑ values for a cross-section with ellipticity $c = 1.5$ and triangularity $\tau = -0.25$. The Mach number is constant, $M = 0.6$, as is the derivative of the Bernoulli function, $\hat{H}' = 1$.

the straight field line coordinate ϑ is constructed by

$$\vartheta = 2\pi \frac{B_z(\psi)}{Z(\psi)} \int \frac{1}{\|\boldsymbol{\nabla}\psi\|}\, dl. \tag{2.14}$$

Here the integration is along the poloidal arclength. In this way, the Jacobian is a flux function $J = J(\psi)$, as is the winding number $\nu(\psi)$.

2.1. Examples of stationary states

Although the FLES code can handle general up–down-symmetric boundaries, we restrict ourselves in this chapter to boundaries that can be described by an ellipticity c and a triangularity τ:

$$x = \cos(\gamma + \tau \sin\gamma), \qquad y = c \sin\gamma, \tag{2.15}$$

where $0 \leqslant \gamma \leqslant \pi$. First, consider an elliptical cross-section ($\tau = 0$). When the profiles for M and $\hat{H}'$ are constant, (2.2) can be solved analytically:

$$\psi = x^2 + \left(\frac{y}{c}\right)^2, \qquad c \equiv \frac{b}{a}. \tag{2.16}$$

Note that we have scaled the flux with the flux at the boundary. The current density is constant and equal to $j_z = 2(1+1/c^2)$, and the poloidal magnetic field and velocity have a linear radial dependence. The Jacobian reduces to a constant: $J(\psi) = \frac{1}{2}c$.

In Fig. 1, flux surfaces of the solution for an ellipticity of 1.5 and a triangularity of -0.25 are shown for $M = 0.6$ and $\hat{H}' = 1$. The magnetic axis is slightly moved owing to the triangularity. However, since the plasma is incompressible, this effect is small compared with that in compressible plasmas. Furthermore, compared with the purely elliptical case, the triangularity increases the strength of the poloidal magnetic field. This is shown in Fig. 2, where the Jacobian, i.e. the inverse of the poloidal magnetic field strength, is plotted.

The FLES code is not restricted to constant input profiles. The profiles for the

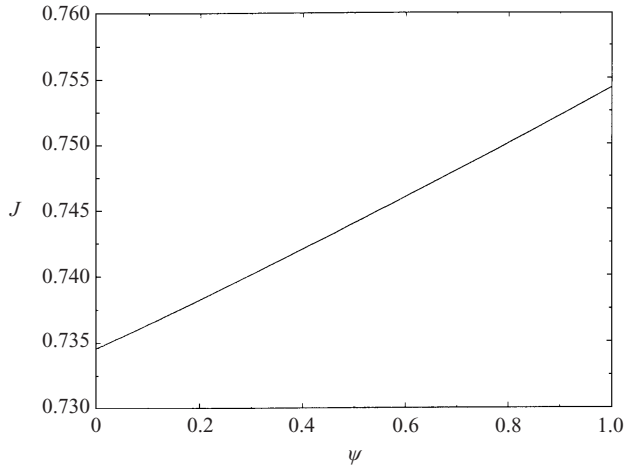

Figure 2. The Jacobian function for the same equilibrium as for Fig. 1.

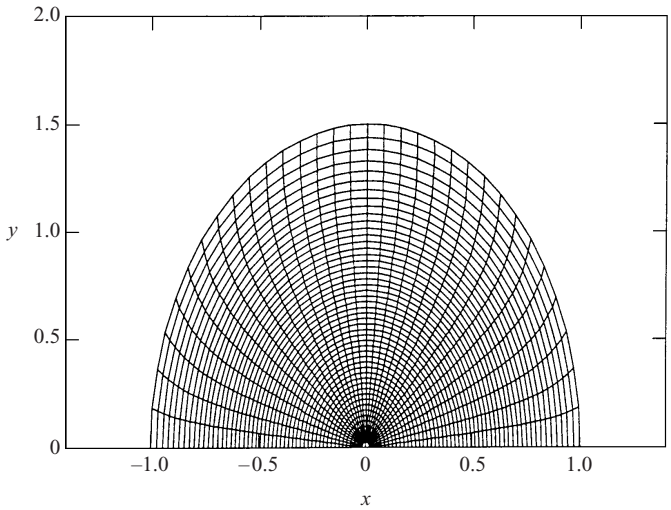

Figure 3. Flux surfaces and equidistant ϑ values for an elliptical cross-section, $c = 1.5$, and non-constant profiles. The Mach number is quadratic in ψ, $M = 0.2\psi^2$, and the derivative of the Bernoulli function is fourth order in ψ, $\hat{H}' = 1 - 1.9\psi^2 + 0.9\psi^4$.

Mach number M and the derivative $\hat{H}'$ of the Bernoulli function, may have arbitrary shape, except that the right hand side of equation (2.6) must be small enough for the Picard iteration to converge. This means, for instance, that the Mach number may not cross the value $M = 1$. As an example of an equilibrium for non-constant input profiles, we show a 'tokamak-like' equilibrium. For a quadratic Mach-number profile, $M = 0.2\psi^2$, a fourth-order profile for the derivative of the Bernoulli function, $\hat{H}' = 1 - 1.9\psi^2 + 0.9\psi^4$, and an elliptical cross-section, the flux surfaces are shown in Fig. 3. The lines of equidistant ϑ are curved towards the edge of the cylinder, whereas they remain straight for constant input profiles. This can also be seen from Fig. 4(a), where the non-constant Jacobian is shown.

Figure 4(b) shows the current density averaged over a flux surface as a function of

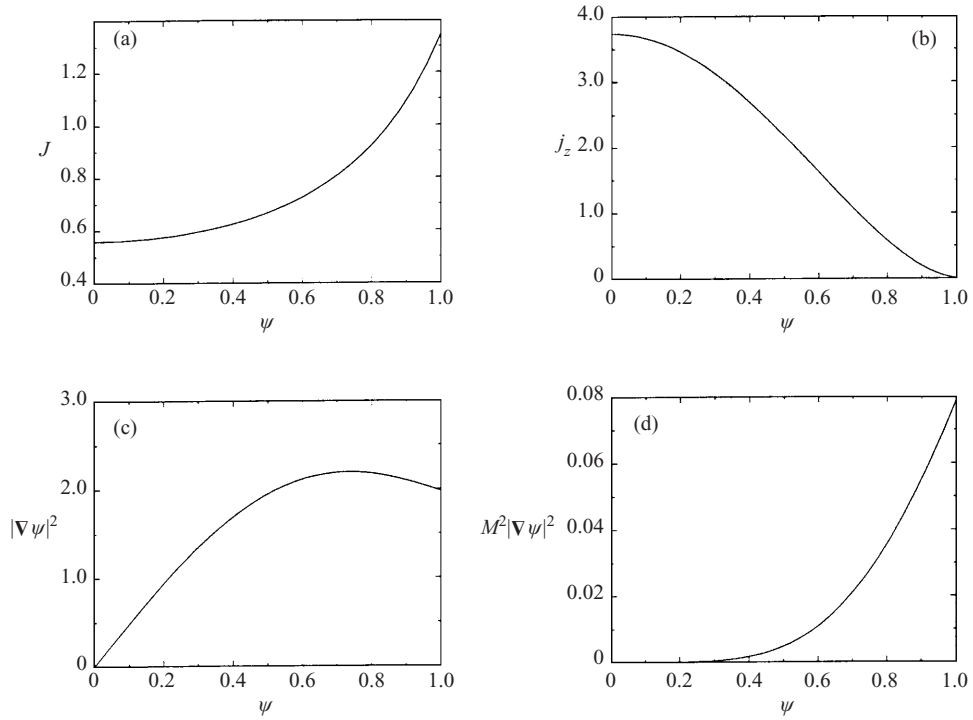

Figure 4. Equilibrium profiles for the same parameters as Fig. 3: (a) the Jacobian function; (b) the current density averaged over a flux surface; (c) the square of the strength of the poloidal magnetic field at $y = 0$; (d) the square of the strength of the poloidal velocity at $y = 0$.

the magnetic flux. Plots (c) and (d) show the squares of the poloidal magnetic field and of the poloidal flow as functions of the magnetic flux. The current density is maximal at the core of the cylinder, and falls off to zero near the edge. The poloidal magnetic field strength increases radially first, but then decreases somewhat near the edge. The poloidal flow is localized near the edge. Therefore this equilibrium may be seen to model a tokamak with an on-axis current and an edge flow.

3. Waves and instabilities

In order to determine whether the calculated equilibria of the previous section are exponentially stable, we developed a numerical code to calculate the spectrum of these incompressible plasma cylinders. The structure of the code is similar to that of the CASTOR code for calculating the spectra of a static compressible torus (Huysmans et al. 1993, Kerner et al. 1998).

3.1. Linear perturbations

For the calculation of waves and instabilities, the incompressible MHD equations are linearized around a stationary equilibrium. For the perturbations, we consider normal modes and a Fourier series in the longitudinal direction. Hence all quantities have the form

$$f(\mathbf{x}, t) = f_0(s, \vartheta) + e^{\sigma t} \int f_1(s, \vartheta; k_z) e^{ik_z z}\, dk_z, \tag{3.1}$$

where $s = \psi^{1/2}$. The variable σ is related to the wave frequency ω by $\sigma = -i\omega$. Using this expansion, the linearized incompressible MHD equations take the form

$$\sigma\rho_1 = -\mathbf{V}_0 \cdot \boldsymbol{\nabla}\rho_1 - \mathbf{v}_1 \cdot \boldsymbol{\nabla}\rho_0, \tag{3.2}$$

$$\begin{aligned}\sigma\rho_0\mathbf{v}_1 = &-\rho_0\mathbf{V}_0 \cdot \boldsymbol{\nabla}\mathbf{v}_1 - \rho_0\mathbf{v}_1 \cdot \boldsymbol{\nabla}\mathbf{V}_0 - \rho_1\mathbf{V}_0 \cdot \boldsymbol{\nabla}\mathbf{V}_0 \\ &+(\boldsymbol{\nabla} \times \mathbf{A}_1) \cdot \boldsymbol{\nabla}\mathbf{B}_0 + \mathbf{B}_0 \cdot \boldsymbol{\nabla}(\boldsymbol{\nabla} \times \mathbf{A}_1) - \boldsymbol{\nabla}\pi_1,\end{aligned} \tag{3.3}$$

$$\sigma\mathbf{A}_1 = \mathbf{V}_0 \times (\boldsymbol{\nabla} \times \mathbf{A}_1) + \mathbf{v}_1 \times \mathbf{B}_0, \tag{3.4}$$

$$0 = \boldsymbol{\nabla} \cdot \mathbf{v}_1. \tag{3.5}$$

All quantities with a subscript 0 are equilibrium quantities, and all quantities with a subscript 1 are first-order perturbations. Furthermore, π_1 is the perturbed total pressure and $\mathbf{A}_1$ is the vector potential of the perturbed magnetic field.

One of the problems of the numerical solution of the eigenvalue problem is that the perturbed magnetic field and perturbed velocity must be divergence-free. This condition for the magnetic field is fulfilled by introducing a vector potential. Faraday's law is integrated, and yields an evolution equation for the vector potential (3.4). In this way, an extra eigenvalue zero is introduced, but this eigenvalue is easily filtered out afterwards.

A similar procedure as for the magnetic field does not work for the velocity perturbation, since it is not possible to integrate the linearized momentum equation (3.3). Therefore we use another method for the velocity. Instead of solving the divergence-free condition (3.5) we replace this equation with an eigenvalue equation (Zienkiewicz 1971)

$$\sigma\pi_1 = Z\boldsymbol{\nabla} \cdot \mathbf{v}_1. \tag{3.6}$$

Here Z is a large number (typically of order 10^6 in the code).

Equations (3.2)–(3.4) and (3.6) describe an approximate eigenvalue problem for incompressible perturbations. The divergence-free condition is replaced by an eigenvalue equation that can be treated the same way as the other equations. In this way, an extra eigenvalue of the order of Z is introduced, which is again easily filtered out afterwards. The other eigenvalues are approximations of the eigenvalue solutions of the original incompressible problem, where the error is of the order of $1/Z$. Hence an approximation of the eigenvalues up to any accuracy needed may be found.

3.2. The IN2FLES code

For the solution of the eigenvalue system (3.2)–(3.6), we developed a code called IN2FLES (Incompressible 2-dimensional plasma FLow Eigenvalue Solver). This code is based on the CASTOR code for the calculation of the resistive MHD spectrum of static toroidal plasmas. The Galerkin method is applied in combination with a finite-element discretization for the radial direction and a Fourier decomposition for the poloidal direction. For details about the numerics, we refer to Huysmans et al. (1993) and Kerner et al. (1998). Here we describe the code for the incompressible plasma cylinder globally, and we point out where the new code differs from CASTOR.

We use (s, ϑ, z) as coordinates, where s is a function of ψ and (ψ, ϑ, z) are the coordinates in which the equilibrium is known. The non-zero metric coefficients g^{ij}

and g_{ij} are then given by:

$$g^{11} = \|\boldsymbol{\nabla} s\|^2 = \frac{1}{f^2}\|\boldsymbol{\nabla}\psi\|^2, \tag{3.7}$$

$$g^{12} = \boldsymbol{\nabla} s \cdot \boldsymbol{\nabla}\vartheta = \frac{1}{f}\boldsymbol{\nabla}\psi \cdot \boldsymbol{\nabla}\vartheta, \tag{3.8}$$

$$g^{22} = \|\boldsymbol{\nabla}\vartheta\|^2, \tag{3.9}$$

$$g^{33} = \|\boldsymbol{\nabla} z\|^2 = 1, \tag{3.10}$$

and

$$g_{11} = f^2 J^2 \|\boldsymbol{\nabla}\vartheta\|^2, \tag{3.11}$$

$$g_{12} = -f^2 J^2 \boldsymbol{\nabla} s \cdot \boldsymbol{\nabla}\vartheta = -f J^2 \boldsymbol{\nabla}\psi \cdot \boldsymbol{\nabla}\vartheta, \tag{3.12}$$

$$g_{22} = f^2 J^2 \|\boldsymbol{\nabla} s\|^2 = J^2 \|\boldsymbol{\nabla}\psi\|^2, \tag{3.13}$$

$$g_{33} = 1, \tag{3.14}$$

where

$$\boldsymbol{\nabla}\psi = f(s)\boldsymbol{\nabla} s,$$

with an arbitrary function $f(s)$ used for grid accumulation. A convenient choice made in the code is $s = \psi^{1/2}$, so that $f = 2s$. The metric coefficients are calculated numerically from the equilibrium solution.

For the perturbations, we use the variables

$$\mathbf{v}_1 = \frac{1}{fJ}(\bar{v}_1 \mathbf{u}^1 - i\bar{v}_2 \mathbf{u}^2 - i\bar{v}_3 \mathbf{u}^3), \tag{3.15}$$

$$\mathbf{A}_1 = -i\bar{A}_1 \mathbf{u}_1 + \bar{A}_2 \mathbf{u}_2 + \bar{A}_3 \mathbf{u}_3. \tag{3.16}$$

Hence the perturbed velocity is represented basically contravariantly and the perturbed vector potential basically covariantly. Furthermore, the perturbed density and the perturbed total pressure are scaled as follows:

$$\bar{\rho}_1 = fJ\rho_1, \qquad \bar{\pi}_1 = fJ\pi_1. \tag{3.17}$$

The variables $(\bar{\rho}_1, \bar{v}_1, \bar{v}_2, \bar{v}_3, \bar{\pi}_1, \bar{A}_1, \bar{A}_2, \bar{A}_3)$ depend on the radial coordinate s and the poloidal coordinate ϑ. For the longitudinal direction z, one Fourier mode is considered, since these modes do not couple. The radial direction is discretized using a finite-element method. In order to avoid poor resolution of the eigenvalues or extra spurious eigenvalues ('spectral pollution'), $\bar{v}_1$, $\bar{A}_2$ and $\bar{A}_3$ are discretized using cubic elements, whereas the other variables are discretized using quadratic elements (Rappaz 1977). For the poloidal direction, a Fourier decomposition is made, where the different modes will couple owing to geometric effects.

For a perfectly conducting wall at the plasma boundary, the normal component of the velocity and of the magnetic field as well as the tangential components of the electric field must vanish at this boundary. This leads to the following boundary conditions:

$$\bar{v}_1\big|_{\text{wall}} = 0, \qquad \bar{A}_2\big|_{\text{wall}} = 0, \qquad \bar{A}_3\big|_{\text{wall}} = 0. \tag{3.18}$$

Regularity of the solution at the magnetic axis yields

$$\bar{v}_1\big|_{\text{axis}} = 0, \qquad \bar{A}_2\big|_{\text{axis}} = 0, \qquad \bar{A}_3\big|_{\text{axis}} = 0. \tag{3.19}$$

These are the six boundary conditions that are applied in the CASTOR code. In

CASTOR, resistive perturbations are considered, which makes the system of sixth order. Here, ideal perturbations are considered, and hence the system of equations is of second order. Therefore only two boundary conditions will be needed. Imposing the boundary conditions (3.18) and (3.19) is consistent, since it can be shown that the three conditions at the wall are dependent and yield only one independent condition, and the same holds for the conditions on the axis. Hence exactly two independent conditions are applied as needed.

The Galerkin method in combination with a mixed finite-element–Fourier discretization applied to (3.2)–(3.6) leads to a very large matrix eigenvalue problem. The analogous problem for one-dimensional geometries is solved using a QR solver and an inverse vector iteration method as described by Nijboer et al. (1997b). However, for two-dimensional problems, these solvers are quite limiting. Using a QR solver for the two-dimensional problem allows one only to take a few Fourier modes into consideration. The use of a high number of Fourier modes is not possible because of memory restrictions. In general, the number of Fourier modes that one is able to include when using a QR solver is not enough to find a converged spectrum. On the other hand, the use of an inverse vector iteration method allows one to find only a single eigenvalue at a time, and it is therefore not suited for the calculation of a complete spectrum.

Because of the restrictions on the QR and inverse vector iteration methods, we solve the matrix eigenvalue problem with a Jacobi–Davidson solver (Sleijpen and Van der Vorst 1996; Nool and Van der Ploeg 1998). This is a new iterative solver that in one run solves for a number of eigenvalues situated in the neighbourhood of a given value. Hence it is very well suited for these large eigenvalue problems. It allows for much larger problems than can be handeled with a QR solver. For the present studies we used 50–100 radial grid points and up to 20 poloidal harmonics, which is enough to find an accurate spectrum. Typically 10 spectral values are found at a time, and this allows one to construct a large part of the spectrum in a few runs. Results are presented in Sec. 5.

4. Continuous spectrum for linear plasma equilibria

Before we start the numerical investigation of the discrete spectrum, it is important to consider the continuous part of the spectrum. First, this is because it contains possible cluster points for the discrete spectrum, and therefore gives an indication of where to find the discrete spectrum. Secondly, the continuous part of the spectrum is interesting in its own right. As pointed out by Hameiri and Hammer (1979) and Hellsten and Spies (1979), the continuous part of the spectrum may turn overstable for flowing plasmas in two-dimensional geometries. Since the continuous spectrum allows a further analytical treatment, we aim to calculate this part of the spectrum explicitly for an elliptical cylinder with a constant current density.

4.1. Continuum equations

In this subsection, we consider the poloidal Mach number M to be constant and the Bernoulli function to be linear in ψ. For this case, the modified Grad–Shafranov equation reduces to a Poisson equation, whose solution is given by (2.16). We choose the remaining functions ρ, B_z and V_z to be constant.

Introduce the incompressible Lagrangian displacement vector $\boldsymbol{\xi}$,

$$\mathbf{v}_1 \equiv \sigma\boldsymbol{\xi} + \mathbf{V}_0 \cdot \boldsymbol{\nabla}\boldsymbol{\xi} - \boldsymbol{\xi} \cdot \boldsymbol{\nabla}\mathbf{V}_0, \tag{4.1}$$

and project this vector normally to the flux surfaces, ξ_n, tangentially to the flux surfaces, ξ_t, and along the longitudinal direction, ξ_z. Then the linearized MHD equations reduce to the form

$$\frac{1}{c}(c^2\cos^2\vartheta+\sin^2\vartheta)^{1/2}\frac{\partial}{\partial s}\begin{pmatrix}\xi_n\\ \pi_1\end{pmatrix}+\mathbf{B}\begin{pmatrix}\xi_n\\ \pi_1\end{pmatrix}+\mathbf{C}\begin{pmatrix}\xi_t\\ \xi_z\end{pmatrix}=0, \tag{4.2}$$

$$\mathbf{D}\begin{pmatrix}\xi_n\\ \pi_1\end{pmatrix}+\mathbf{E}\begin{pmatrix}\xi_t\\ \xi_z\end{pmatrix}=0, \tag{4.3}$$

where $s=\psi^{1/2}$. $\mathbf{B}$, $\mathbf{C}$, $\mathbf{D}$ and $\mathbf{E}$ are 2×2 matrices that depend on the equilibrium quantities s, ϑ and ∂_ϑ, but not on ∂_s. Since the matrix operators $\mathbf{B}$, $\mathbf{C}$, $\mathbf{D}$ and $\mathbf{E}$ depend on ϑ, the different poloidal modes will couple. It follows from the expressions given in the Appendix that only modes with difference $\Delta m=2$ couple.

The system of equations (4.2), (4.3) can be solved by using (4.3) to express ξ_t and ξ_z in terms of ξ_n and π_1 and substituting these expressions into (4.2). This procedure will work whenever the operator $\mathbf{E}$ is invertible. The continuous part of the spectrum (the cluster points) comprises those values of σ for which the matrix operator $\mathbf{E}$ is not invertible (Hameiri and Hammer 1979; Kieras and Tataronis 1982).

Here the matrix operator $\mathbf{E}$ is diagonal, and the equations describing the cluster points are

$$\left\{(M^2-1)\frac{1}{J^2}\frac{\partial^2}{\partial\vartheta^2}+2\,(M\sigma-ik_zB_z)\,\frac{1}{J}\frac{\partial}{\partial\vartheta}+\sigma^2+k_z^2B_z^2 \right.$$
$$\left.+(M^2-1)\frac{1}{J^2}\left[1-\frac{c^2}{(c^2\cos^2\vartheta+\sin^2\vartheta)^2}\right]\right\}\xi_t=0, \tag{4.4}$$

$$\left[(M^2-1)\,\frac{1}{J^2}\frac{\partial^2}{\partial\vartheta^2}+2\,(M\sigma-ik_zB_z)\,\frac{1}{J}\frac{\partial}{\partial\vartheta}+\sigma^2+k_z^2B_z^2\right]\xi_z=0. \tag{4.5}$$

Since the matrix operator $\mathbf{E}$ is diagonal, the tangential and longitudinal parts of the continuous spectrum decouple. This is a very special feature, which occurs for cylindrical, incompressible plasmas. Equation (4.5) was also found for an X-point geometry, whereas (4.4) is modified because of the difference in field-line curvature (Nijboer et al. 1998).

In general, for two-dimensional compressible plasmas, the continua are coupled. For one-dimensional compressible plasmas, the continua decouple, but only when projected onto the field lines. This projection is here replaced in favour of the symmetry directions. Thus the polarizations of the continua of two-dimensional incompressible and one-dimensional compressible plasmas differ. In the case of a one-dimensional incompressible plasma, the continua are degenerate, so that both types of polarization are valid.

Equation (4.5) for the longitudinal component is a differential equation with constant coefficients, and therefore, all poloidal modes are decoupled. Considering an $\exp(im\vartheta)$ dependence then yields the following dispersion relation:

$$\left(\sigma+\frac{imM}{J}\right)^2+\left(\frac{m}{J}+k_zB_z\right)^2=0. \tag{4.6}$$

This yields the same spectral values as for the circular cylinder.

The tangential component of the continuous spectrum is affected by the non-

circularity of the geometry. In the limit of a circular plasma ($c \to 1$), the poloidal modes are decoupled again, and the tangential component yields the same spectral values as the longitudinal component. Hence these values are degenerate, and any linear combination yields an eigenvector. Thus the incompressible limit of one-dimensional compressible plasmas and the one-dimensional limit of two-dimensional incompressible plasmas coincide.

One may transform (4.4) for the tangential component into a Matthieu equation. Introducing the new variable ζ,

$$\xi_t(\vartheta) = \exp\left[\frac{J(M\sigma - ik_zB_z)}{1-M^2}\vartheta\right]\zeta(\vartheta), \tag{4.7}$$

transforms (4.4) into

$$\left[\frac{\partial^2}{\partial\vartheta^2} - \frac{J^2(\sigma - ik_zB_zM)^2}{(1-M^2)^2} + 1 - \frac{c^2}{(c^2\cos^2\vartheta + \sin^2\vartheta)^2}\right]\zeta = 0. \tag{4.8}$$

Although the solution of ξ_t must be 2π-periodic in ϑ, this does not hold for ζ. In fact, for non-vanishing Mach numbers, the spectral value σ appears both in the Matthieu equation and in the boundary conditions. Since we developed a numerical code for the calculation of the complete spectrum, we shall not investigate this equation further.

4.2. Perturbed continua

In order to provide a check for the numerics, we calculate the effect of the ellipticity on the spectrum explicitly. We shall perturb the geometry only and leave the plasma area constant, so that J keeps the same value. Note that, in this way, the flux at the boundary is perturbed. We assume small ε,

$$\varepsilon = 1 - c^2, \tag{4.9}$$

and write ξ_t as a sum of normal modes:

$$\xi_t = \sum \alpha_m \exp(im\vartheta). \tag{4.10}$$

Substitution of (4.9) and (4.10) into (4.2) yields an infinite set of linear equations for the coefficients α_m.

Writing the spectral value as

$$\sigma = \sigma_0 + \sigma_1\varepsilon + \sigma_2\varepsilon^2 + \mathcal{O}(\varepsilon^3), \tag{4.11}$$

we can distinguish a number of cases. Depending on equilibrium parameters, the spectral value σ_0 may be non-degenerate or it may be degenerate with $\Delta m = 2$ or $\Delta m = 4$, etc. Degeneracies of odd Δm may also occur, but since these modes do not couple in an elliptical cylinder, we may treat them as non-degenerate. Note that for fixed values of k_zB_z and M/J, a fixed value of σ_0 is always either non-degenerate or twofold degenerate. This is a modification of the analysis of Dewar et al. (1974) for static plasmas.

In the case where σ_0 is non-degenerate, i.e.

$$\sigma_0 = -\frac{imM}{J} \pm i\left(\frac{m}{J} + k_zB_z\right) \tag{4.12}$$

for only one value of m, we find that the perturbation of this spectral value due to

ellipticity is of second order: $\sigma_1 = 0$. For σ_2, we find

$$\sigma_2 = \mp \frac{i}{16} \frac{(1-M^2)\left(\frac{m}{J} + k_z B_z\right)}{(1 \pm M)^2 - J^2\left(\frac{m}{J} + k_z B_z\right)^2}. \tag{4.13}$$

Whenever

$$(1 \pm M)^2 > J^2\left(\frac{m}{J} + k_z B_z\right)^2,$$

the modulus of the spectral value is lowered, and for

$$(1 \pm M)^2 < J^2\left(\frac{m}{J} + k_z B_z\right)^2,$$

it is raised. This is in agreement with results by Dewar et al. (1974) for static plasmas.

When σ_0 is degenerate with $\Delta m = 2$, i.e. σ_0 satisfies (4.12) for two different values of m, say m and $m+2$, we find a first-order correction due to ellipticity:

$$\sigma_1^2 = \frac{\frac{(1-M^2)^2}{J^4}}{16\left(\sigma_0 + \frac{2imM}{J}\right)\left[\sigma_0 + \frac{2i(m+2)M}{J}\right]}. \tag{4.14}$$

Hence, the perturbation is symmetric around σ_0, which is in agreement with Dewar et al. (1974). Moreover, it turns out that the background flow may turn these spectral values unstable. In the limit of a purely longitudinal magnetic field and a purely poloidal flow, this agrees with Hameiri and Hammer (1979).

5. The two-dimensional discrete spectrum

In this section, the effect of a non-circular cross-section on the discrete spectrum is discussed. The longitudinal velocity is taken to be constant, and hence it only gives rise to a constant Doppler shift of the complete spectrum. Therefore it can be chosen to be zero without loss of generality. Also, the density is chosen to be constant. Instabilities driven by an unfavourable density profile are not considered here, but are considered by Fung (1984) and Nijboer et al. (1997a). Thus the instabilities that we encounter are either driven by the magnetic field or by the plasma flow.

We start by discussing the spectrum of linear equilibria. For this, the longitudinal magnetic field is chosen to be constant and the geometry has an elliptic cross-section, such that the Jacobian is also constant. In Fig. 5, the complete spectrum for one poloidal harmonic in a circular cylinder ($c = 1$) is shown. This spectrum was calculated using the LEDAFLOW code (Nijboer et al. 1997b) for a circular geometry as a check on the IN2FLES code. Since the equilibrium is one-dimensional, no mode coupling occurs. The static case is shown in Fig. 5(a). The spectrum lies on the real and imaginary axes of the complex σ plane, and is symmetric with respect to these axes. The discrete modes cluster from two sides towards each of the two stable cluster points $\sigma_0 = \pm(\mathbf{k}\cdot\mathbf{B})i$. This is depicted by the arrows. Furthermore, the equilibrium is unstable, since there are discrete modes on the positive real axis. These are magnetic instabilities, which are also known as internal kink instabilities.

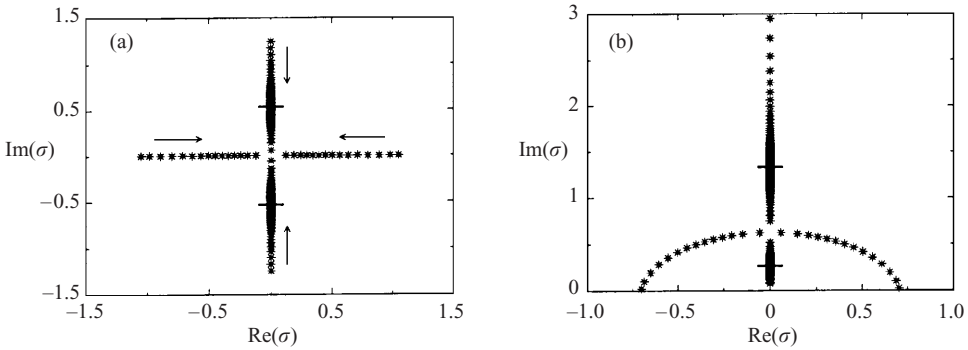

Figure 5. Discrete cluster spectrum for one poloidal mode in a circular geometry: (a) the static case, $M = 0$; (b) a rotating case, $M = 0.6$; $J = 0.75$, $k_z = 10$, $B_z = 0.08$, $m = -1$. The discrete modes are depicted by asterisks and cluster towards the cluster points, which are depicted by horizontal bars. The direction of clustering is indicated by the arrows in (a).

In Fig. 5(b) the same situation is shown but now with a poloidal flow. The discrete spectrum still clusters towards the cluster points, which are Doppler-shifted along the imaginary axis. The spectrum is still symmetric with respect to the imaginary axis, but the symmetry with respect to the real axis is broken. The flow clearly has a stabilizing effect in the sense that the real part of the spectral value σ has diminished. This was also shown by Nijboer et al. (1997a). Furthermore, the damped and unstable modes are shifted into the complex plane, so that the unstable modes now become overstable.

The overstable and damped modes lie on a circle with radius

$$R = \frac{(1 - M^2)^{1/2}}{M} \left| \frac{m}{J} + k_z B_z \right| \tag{5.1}$$

and origin

$$\sigma_0 = -im\frac{M}{J} + \frac{i}{M}\left(\frac{m}{J} + k_z B_z\right). \tag{5.2}$$

This was already shown by Lifschitz (1998), who considered linear equilibria on unbounded domains. The effect of a wall at a finite distance, which we investigate here, is that the continuous curve of spectral values found by Lifschitz discretises into the discrete modes that are shown here. It was also shown by Lifschitz (1998) that, for fixed equilibrium parameters, at least two and at most four poloidal mode numbers give rise to overstable modes. The density of the eigenvalues on the curves depends on k_z. The larger the value of $|k_z|$, the more eigenvalues lie on the curves (Nijboer et al. 1997a). Therefore we can resolve the spectral curves by taking k_z large while keeping $\mathbf{k} \cdot \mathbf{B}$ at a fixed value. The latter can be achieved by changing the poloidal mode number m or by adjusting the longitudinal magnetic field B_z.

The effect of ellipticity on the unstable spectrum is shown in Fig. 6. For the cylindrical case, the spectrum of four modes was calculated: two even modes ($m = -2$ and $m = 0$), for which the unstable spectrum is shown in (a), and two odd modes ($m = -1$ and $m = 1$), for which it is shown in (b). For the spectrum of an elliptical cylinder, even and odd modes were calculated separately using 12 poloidal harmonics for each calculation. The unstable part of the spectrum for the even modes is shown in (c), and for the odd modes it is shown in (d).

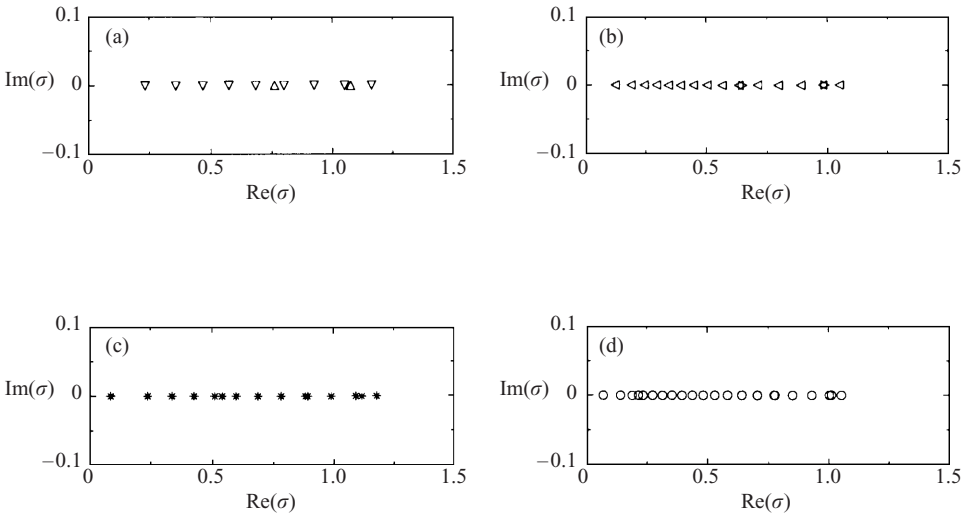

Figure 6. The effect of ellipticity ($c = 1.5$) on the unstable spectrum for a static plasma; $M = 0$, $J = 0.75$, $k_z = 10$, $B_z = 0.08$. Different modes are depicted by different symbols. (a) Circular cross-section: even modes $m = -2$ ($\triangle$), $m = 0$ ($\triangledown$). (b) Circular cross-section: odd modes $m = -1$ ($\triangleleft$), $m = 1$ ($\triangleright$). (c) Elliptical cross-section: even modes ($*$). (d) Elliptical cross-section: odd modes ($\bigcirc$).

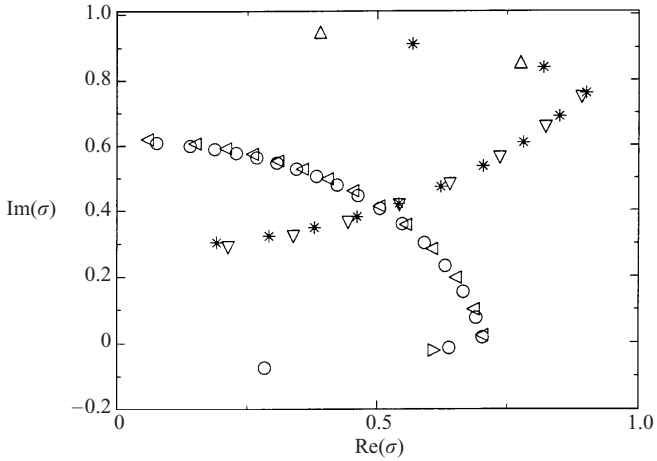

Figure 7. The effect of ellipticity on the overstable spectrum for a rotating plasma, $M = 0.6$. The overstable spectrum is shown for even modes and odd modes in a circular and an elliptical cylinder. The parameters are the same as for Fig. 6, except for the poloidal flow. The symbols also have the same meaning as in Fig. 6.

All spectral values lie on the real axis, since the plasma is static. The ellipticity has a destabilizing effect, in the sense that for each individual eigenvalue the real part of σ has increased. The effect is small, and it is hardly visible for the most unstable modes. However, comparing Fig. 6(a) with 6(c), and 6(b) with 6(d), it is seen that the number of unstable modes has increased. The maximum instability of the total plasma has hardly increased, as can be seen on comparing (a) with (c).

Figure 7 shows the overstable spectrum for the same equilibrium values as for

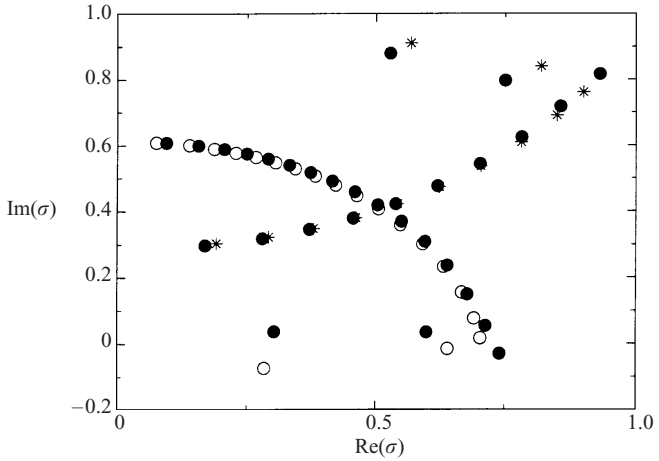

Figure 8. The overstable spectrum corresponding to the equilibrium of Fig. 1 with an ellipticity of $c = 1.5$ and a triangularity of $\tau = -0.25$. The spectral values are depicted by black dots and may be compared with the purely elliptical spectrum of Fig. 7. The parameters are $M = 0.6$, $k_z = 10$ and $B_z = 0.08$.

Fig. 6, but now with the poloidal flow present. As a consequence, the discrete modes shift into the complex plane onto different curves for the different poloidal mode numbers, again shown by triangles for a circular geometry. Even and odd modes are now shown in the same figure. Since different poloidal harmonics m result in different spectral curves, the effect of ellipticity on the spectrum is clearer than for the static case. It is now seen that the ellipticity is destabilizing for each individual mode (i.e., for each mode, the real part of σ has increased). However, the maximum growth rate has hardly changed. Furthermore, the discrete modes remain close to the curves of the circular case. The coupling between modes with a mode difference $\Delta m = 2$ does not affect the curves much. It predominantly changes the position of the eigenvalues on the curves.

In order to further study the effect of coupling on the discrete spectrum, we considered a boundary with ellipticity $c = 1.5$ and triangularity $\tau = -0.25$. Owing to the triangularity, a $\Delta m = 3$ coupling also occurs. This coupling, together with the $\Delta m = 2$ coupling due to the ellipticity, causes all modes to be coupled now. The equilibrium solution is depicted in Fig. 1, and we show the corresponding overstable spectrum in Fig. 8 together with the overstable spectrum for the purely elliptical case of Fig. 7. For the calculation of the spectrum of the geometry with triangularity, 22 poloidal harmonics were used. The dominant $m = -1$ and $m = 0$ curves hardly change in comparison with the purely elliptical case, although the modes on these curves move slightly. Only the endpoints of these curves are affected, such that the plasma becomes more unstable. The dominant $m = -2$ and $m = 1$ curves are affected more, and here we see that the modes are stabilized.

When the triangularity is increased to $\tau = -0.5$, the shear in the magnetic field and the flow is increased, as exhibited by the Jacobian (Fig. 9). The corresponding overstable spectrum is shown in Fig. 10. The dominant $m = -1$ and $m = 0$ are still close to the original curves, but the dominant $m = -2$ and $m = 1$ are now completely gone from their original positions. Round the $m = -1$ and $m = 0$

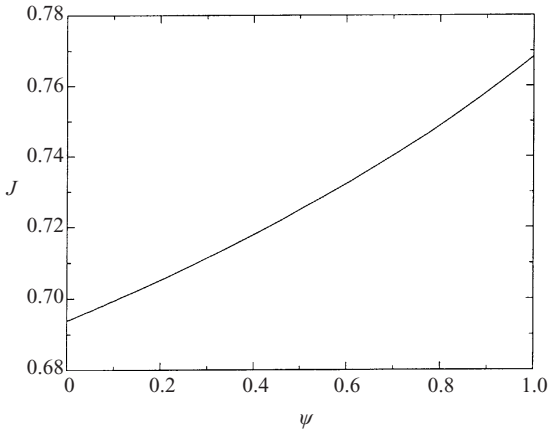

Figure 9. The Jacobian function for a similar equilibrium as used for Fig. 8, but with a triangularity of $\tau = -0.5$.

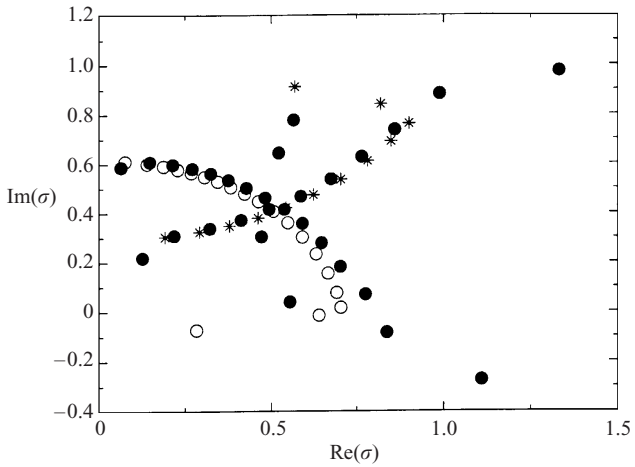

Figure 10. The overstable spectrum corresponding to a similar equilibrium as used for Fig. 8, but for a triangularity of $\tau = -0.5$. The spectral values are depicted by black dots. Also shown are the spectral values for the purely elliptical case, $\tau = 0$, of Fig. 7.

crossing, the modes are affected greatly, and the modes on the end of the $m = -1$ and $m = 0$ curves have turned more unstable.

We end this section by showing a flow-driven instability. In Fig. 11, we show part of the spectrum for an elliptical cross-section. All equilibrium profiles are the same as for Fig. 6, except that $M = 1.15$. It is known for circular incompressible plasmas that the plasma is completely stable in this case (Nijboer et al. 1997a). In Fig. 11, however, an instability is shown that is due to the flow and the non-circular geometry. Since the spectrum is symmetric with respect to the imaginary σ axis, there are also damped modes. On the imaginary axis, a number of cluster points are found, which show up as an increased number of discrete eigenvalues.

When the Mach number is increased, we find that one of the cluster points becomes overstable. This is seen in Fig. 12, where the clustering towards this cluster point is shown for different values of the Mach number. The fact that the cluster

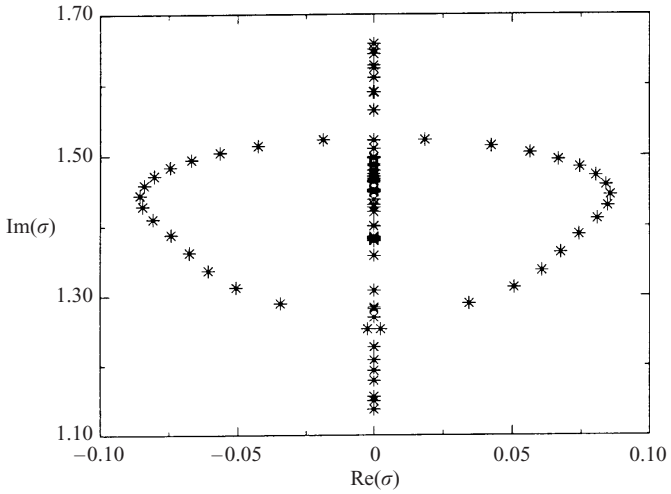

Figure 11. The overstable spectrum for an elliptical cross-section, $c = 1.5$, and parameters $J = 0.75$, $k_z = 10$, $B_z = 0.08$ and $M = 1.15$. Apart from the value of the Mach number, these are the same parameters as used for Fig. 6.

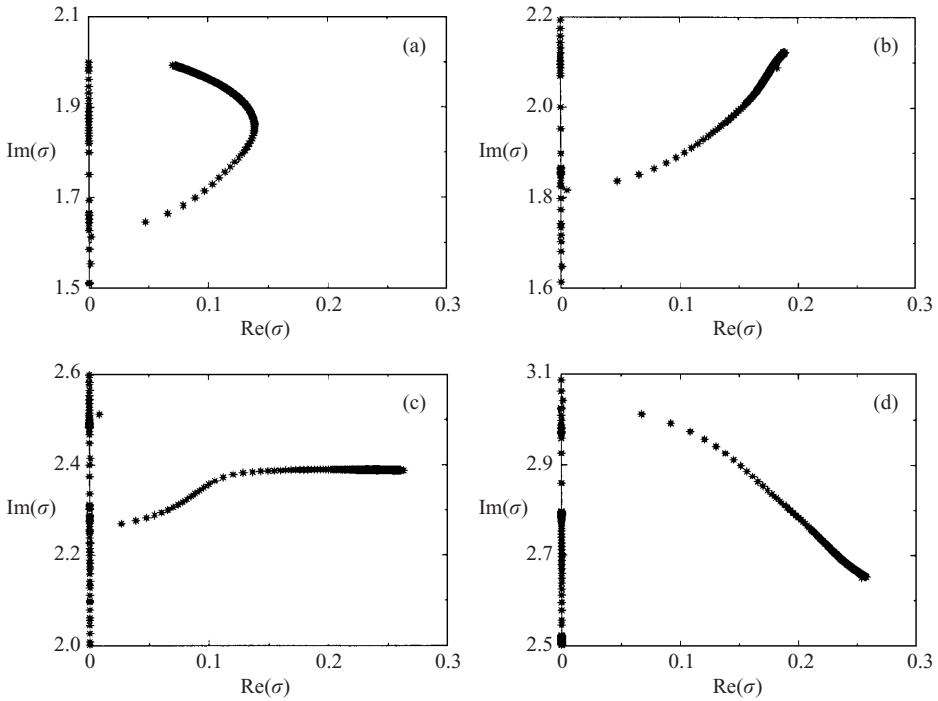

Figure 12. Overstable cluster spectra for an elliptical cross-section. Apart from the value of the Mach number the same parameters are used as for Fig. 11: (a) $M = 1.25$; (b) 1.3; (c) 1.4; (d) 1.5.

point may turn overstable was already shown by Hameiri and Hammer (1979), who considered a plasma cylinder with a purely longitudinal magnetic field. They explain that the periodic driving force of the rotation couples to the Alfvén frequency and turns the cluster point overstable. This is called a parametric instability.

Here we show that, with a poloidal magnetic field, the cluster point may still become overstable. Moreover, we show that this arises from overstable discrete modes (Fig. 11), and turns overstable when the Mach number is increased (Fig. 12). Furthermore, discrete modes clustering towards the cluster point are also found. For increasing Mach number, the curve on which the eigenvalues lie 'turns over', so that the cluster point becomes the mode with the largest growth rate.

Finally, we mention that Lifschitz (1995) also found unstable modes for Mach numbers larger than 1 in a cylinder with non-circular cross-section. However, since those calculations were performed completely in Fourier space, the structure of the unstable curves was not found. In particular, the fact that the cluster point turns overstable was not found in this paper.

6. Conclusions

The magnetohydrodynamic spectrum of waves and instabilities in incompressible flowing plasmas has been investigated for cylindrical geometries with non-circular cross-sections. Since the equilibrium problem is two-dimensional, in general, one has to exploit a numerical solution. For this purpose, the FLES code has been developed. The modified Grad–Shafranov equation is discretized using bicubic Hermite finite elements. This generates equilibrium solutions that are accurate enough for the calculation of the spectrum.

For the calculation of the spectrum, the IN2FLES code has been developed. Combining a finite-element discretization in the radial direction and a Fourier discretization in the poloidal direction generates a large eigenvalue problem. This problem is conveniently solved using a Jacobi–Davidson iterative solver.

The continuous part of the spectrum may be investigated analytically further than is possible for the discrete part of the spectrum. This investigation has been performed for linear equilibria. It is found that for incompressible cylindrical geometries, this part of the spectrum decouples into a longitudinal part and a tangential part. For the longitudinal part, all poloidal harmonics are decoupled. This part of the spectrum does not depend on the cross-section, and is the same as the one-dimensional incompressible continuum. This one-dimensional continuum is, however, degenerate. When the cross-section is non-circular, the poloidal harmonics of the tangential component couple, and the degeneracy is lifted.

Perturbation of the circular cross-section with a small ellipticity allows one to calculate the coupling between the different poloidal harmonics of the tangential component explicitly. Whenever the unperturbed spectral value is non-degenerate for different poloidal harmonics, the change is of second order in the perturbation, and is always stable. However, when the unperturbed spectral value is degenerate, its change is of first order in the perturbation, and may lead to an unstable continuous spectrum or cluster point.

The possible effects of such an overstable continuum are as yet unclear. For instance, it may have effects on continuum heating. Since the mode is overstable, it oscillates with increasing amplitude. Therefore the equilibrium may not survive long enough for heating to be effective. However, nonlinear effects may saturate

the growth so that the effects become unpredictable. Further research into this overstable continuum is needed.

On unbounded domains there exists a second type of continuous spectrum. This is a dense set of eigenvalues that discretizes when a wall at a finite distance is introduced. For closed flux surfaces, the discrete modes cluster towards a cluster point, which was termed the 'classical' continuum by Nijboer et al. (1998).

Starting with a linear equilibrium in a circular geometry, the effect of non-circularity has been investigated. The introduction of ellipticity couples all even modes and all odd modes. Every individual mode is destabilized, but the maximum growth rate is not increased much. When triangularity is added, all modes couple. Moreover, the equilibrium can no longer be linear, and shear in the magnetic field and flow velocity follows. This causes some branches of the spectrum to be destabilized, and others to be stabilized. The overall instability of the plasma is thus increased. However, the destabilizing effect of the geometry can be compensated by introducing a stronger poloidal flow.

Apart from the magnetic instability, an instability driven by the flow has been found. This instability was found for $M^2 > 1$, and only exists for non-circular cross-sections. The discrete overstable modes cluster towards an unstable cluster point, which corresponds to the most unstable mode for high enough M.

Acknowledgements

We thank Bart van der Holst and Sander Beliën for many discussions about the HELENA and CASTOR codes, and Auke van der Ploeg for his help with the Jacobi–Davidson solver.

This work was performed as part of the research programme of the Stichting voor Fundamenteel Onderzoek der Materie (FOM), with financial support from the Nederlandse Organisatie voor Wetenschappelijk Onderzoek (NWO). Computing facilities were provided by the Stichting Nationale Computer Facaliteiten (NCF).

Appendix. Linearized equations

For linear equilibria in elliptical geometries with constant density, the equations describing the perturbations from equilibrium reduce to

$$\left(\rho_0^{1/2}\sigma + \frac{M}{J}\mathscr{D}\right)^2 \boldsymbol{\xi} - \left(\frac{1}{J}\mathscr{D} + ik_z B_z\right)^2 \boldsymbol{\xi} + \frac{1}{J^2}(M^2-1)\boldsymbol{\xi}_\perp + \boldsymbol{\nabla}\pi_1 = 0, \tag{A 1}$$

$$\boldsymbol{\nabla}\cdot\boldsymbol{\xi} = 0. \tag{A 2}$$

Here M, $\rho_0 = 1$ and B_z are chosen to be constant, and the fact that the equilibrium is linear results in a constant value of $J = \frac{1}{2}c$. The equilibrium is described in Sec. 2. The system (A 1), (A 2) is equivalent to that for X-point geometries as described by Nijboer et al. (1998).

$\mathscr{D} \equiv \partial_\vartheta$ is the differential operator in the flux surfaces. Hence the only derivatives over the flux surfaces result from the $\boldsymbol{\nabla}\pi_1$ term in (A 1) and (A 2). Writing the equations explicitly yields the system of Sec. 4, where the matrix differential operators $\mathbf{B}$, $\mathbf{C}$, $\mathbf{D}$ and $\mathbf{E}$ read

$$B_{11} = \frac{1}{cs}\frac{\partial p}{\partial\vartheta}\frac{\partial}{\partial\vartheta} + \frac{c}{sp^3}, \tag{A 3}$$

$$B_{12} = 0, \tag{A 4}$$

$$B_{21} = \left(M^2-1\right)\frac{1}{J^2}\frac{\partial^2}{\partial\vartheta^2} + 2\left(M\sigma - ik_zB_z\right)\frac{1}{J}\frac{\partial}{\partial\vartheta} + \sigma^2 + k_z^2B_z^2 + \left(M^2-1\right)\left(\frac{1}{J^2} - \frac{c^2}{J^2p^4}\right), \tag{A 5}$$

$$B_{22} = \frac{1}{cs}\frac{\partial p}{\partial\vartheta}\frac{\partial}{\partial\vartheta}, \tag{A 6}$$

$$C_{11} = \frac{1}{sp}\frac{\partial}{\partial\vartheta} - \frac{1}{s}\frac{\partial}{\partial\vartheta}\left(\frac{1}{p}\right), \tag{A 7}$$

$$C_{12} = ik_z, \tag{A 8}$$

$$C_{21} = -2\left(M\sigma - ik_zB_z\right)\frac{c}{Jp^2} - \left(M^2-1\right)\left[\frac{1}{J^2}\left(\frac{\partial}{\partial\vartheta}\frac{c}{p^2}\right) + \frac{2c}{J^2p^2}\frac{\partial}{\partial\vartheta}\right], \tag{A 9}$$

$$C_{22} = 0, \tag{A 10}$$

$$D_{11} = -C_{21}, \tag{A 11}$$

$$D_{12} = \frac{1}{sp}\frac{\partial}{\partial\vartheta}, \tag{A 12}$$

$$D_{21} = 0, \tag{A 13}$$

$$D_{22} = ik_z, \tag{A 14}$$

$$E_{11} = B_{21}, \tag{A 15}$$

$$E_{12} = 0, \tag{A 16}$$

$$E_{21} = 0, \tag{A 17}$$

$$E_{22} = \left(M^2-1\right)\frac{1}{J^2}\frac{\partial^2}{\partial\vartheta^2} + \left(M\sigma - ik_zB_z\right)\frac{1}{J}\frac{\partial}{\partial\vartheta} + \sigma^2 + k_z^2B_z^2, \tag{A 18}$$

and

$$p(\vartheta) = \left(c^2\cos^2\vartheta + \sin^2\vartheta\right)^{1/2}.$$

Note that the strength of the poloidal magnetic field is given by

$$\|\mathbf{B}_p\| = \frac{s}{J}p(\vartheta). \tag{A 19}$$

Since the coefficients of the system of differential equations (A 1), (A 2) are either constant or π-periodic, only modes with difference $\Delta m = 2$ couple.

References

Agim, Y. Z. and Tataronis, J. A. 1985 General two-dimensional magnetohydrodynamic equilibria with mass flow. *J. Plasma Phys.* **34**, 337–360.

Appl, S. and Camenzind, M. 1992 The stability of current-carrying jets. *Astron. Astrophys.* **256**, 354–370.

Balbus, S. A. and Hawley, J. F. 1998 Instability, turbulence, and enhanced transport in accretion disks. *Rev. Mod. Phys.* **70**, 1–53.

Bodo, G., Rosner, R., Ferrari, A. and Knobloch, E. 1989 On the stability of magnetized jets: the axisymmetric case. *Astrophys. J.* **341**, 631–649.

Bondeson, A., Iacono, R. and Bhattacharjee, A. 1987 Local magnetohydrodynamic instabilities of cylindrical plasmas with sheared equilibrium flows. *Phys. Fluids* **30**, 2167–2180.

Dewar, R. L., Grimm, R. C., Johnson, J. L., Greene, E. A. and Rutherford, P. H. 1974 Long-wavelength kink instabilities in low-pressure, uniform axial current, cylindrical plasmas with elliptic cross sections. *Phys. Fluids* **17**, 930–938.

Fung, Y. T. 1984 On the stability of vortex motions in the presence of magnetic fields. *Phys. Fluids* **27**, 838–847.

Goedbloed, J. P. and Lifschitz, A. E. 1997 Stationary symmetric magnetohydrodynamic flows. *Phys. Plasmas* **4**, 3544–3564.

Hameiri, E. 1981 Spectral estimates, stability conditions, and the rotating screw-pinch. *J. Math. Phys.* **22**, 2080–2088.

Hameiri, E. and Hammer, J. H. 1979 Unstable continuous spectrum in magnetohydrodynamics. *Phys. Fluids* **22**, 1700–1706.

Hellsten, T. A. K. and Spies, G. O. 1979 Continuous magnetohydrodynamic spectrum in axially symmetric rotating plasmas. *Phys. Fluids* **22**, 743–746.

Huysmans, G. T. A., Goedbloed, J. P. and Kerner, W. 1991 Isoparametric bicubic Hermite elements for solution of the Grad–Shafranov equation. In: *Proceedings of the CP90 Conference on Computational Physics* (ed. A. Tenner), pp. 371–376. World Scientific, Singapore.

Huysmans, G. T. A., Goedbloed, J. P. and Kerner, W. 1993 Free boundary resistive modes in tokamaks *Phys. Fluids* **B5**, 1545–1558.

Kerner, W., Goedbloed, J. P., Huijsmans, G. T. A., Poedts, S. and Schwartz, E. 1998 CASTOR: Normal-mode analysis of dissipative MHD plasmas. *J. Comput. Phys.* **142**, 271–303.

Kieras, C. E. and Tataronis, J. A. 1982 The shear Alfvén continuous spectrum of axisymmetric toroidal equilibria in the large aspect ratio limit. *J. Plasma Phys.* **28**, 395–414.

Lifschitz, A. 1995 Exact description of the spectrum of elliptical vortices in hydrodynamics and magnetohydrodynamics. *Phys. Fluids* **7**, 1626–1634.

Lifschitz, A. 1998 A nonlinear spectral problem with periodic coefficients occurring in magnetohydrodynamic stability theory. In: *Proceedings of the 1995 International Workshop on Operator Theory and Applications* (ed. R. Mennicken and C. Tretter), pp. 97–117. Birkhaüser, Boston.

Nijboer, R. J., Lifschitz, A. and Goedbloed, J. P. 1997a Spectrum and stability of a rigidly rotating compressible plasma. *J. Plasma Phys.* **58**, 101–121.

Nijboer, R. J., Van der Holst, B., Poedts, S. and Goedbloed, J. P. 1997b Calculating magnetohydrodynamic flow spectra. *Comput. Phys. Commun.* **106**, 39–52.

Nijboer, R. J., Goedbloed, J. P. and Lifschitz, A. 1998 The spectrum of MHD flows about X points. *J. Plasma Phys.* **60**, 421–446.

Nool, M. and Van der Ploeg, A. 1998 A parallel Jacobi–Davidson method for solving generalized eigenvalue problems in linear magnetohydrodynamics. Submitted.

Rappaz, J. 1977 Approximation of the spectrum of a non-compact operator given by the magnetohydrodynamic stability of a plasma. *Numer. Math.* **28**, 15–24.

Sleijpen, G. L. G. and Van der Vorst, H. A. 1996 A Jacobi–Davidson iteration method for linear eigenvalue problems. *SIAM J. Matrix Anal. Appl.* **17**, 401–425.

Zienkiewicz, O. C. 1971 *The Finite Element Method*, 3rd edn. McGraw-Hill, London.